Hindawi
International Journal of Antennas and Propagation
Volume 2019, Article ID 8421809, 12 pages
https://doi.org/10.1155/2019/8421809

Research Article

High-Gain Quad Array of Nonuniform Helical Antennas

Jelena Lj. Dinkić,[1] Dragan I. Olćan,[1] Antonije R. Djordjević,[1,2] and Alenka G. Zajić[3]

[1]*School of Electrical Engineering, University of Belgrade, 11120 Belgrade, Serbia*
[2]*Serbian Academy of Sciences and Arts, 11000 Belgrade, Serbia*
[3]*School of Electrical and Computer Engineering, Georgia Institute of Technology, Atlanta, GA 30332, USA*

Correspondence should be addressed to Dragan I. Olćan; olcan@etf.bg.ac.rs

Received 25 November 2018; Accepted 20 January 2019; Published 28 March 2019

Academic Editor: Paolo Burghignoli

We present a design of a high-gain quad array of nonuniform helical antennas. The design is obtained by optimization of a 3-D numerical model of four nonuniform helical antennas placed above a ground plane, including a model of a feeding network, utilizing the method of moments with higher-order basis functions. The gain of one optimal nonuniform helical antenna can be about 2.5 dB higher than the gain of a uniform helical antenna of the same axial length. Creating a 2×2 array further increases the gain up to about 6 dB. The resulting quad array fits into a box whose dimensions are $2.5 \times 3.3 \times 3.3$ wavelengths, and the gain in the main radiating direction is about 20.5 dBi in the frequency range from 0.9 GHz to 1.1 GHz. The design is verified by measurements of a prototype of the quad array.

1. Introduction

Helical antennas have been known for more than 70 years [1]. They have been widely used due to their characteristics in the axial radiating mode: almost circularly polarized wave in a reasonably wide frequency band and a relatively simple structure.

Various guidelines for the design of uniform and nonuniform helical antennas are presented in the literature. A systematic investigation with a reliable procedure for designing the geometry of uniform helical antennas is presented in [2].

Optimally designed nonuniform helical antennas have better properties than uniform helical antennas of the same size. For example, [3] proposes the design of compact nonuniform antennas, which do not have a ground plane or a reflector and whose gain surpasses the gain of uniform antennas. The design of nonuniform helical antennas has more degrees of freedom compared to the design of uniform helical antennas. Therefore, designing nonuniform helical antennas of desired characteristics is a challenging task. To find the optimal design of nonuniform helical antennas, various optimization algorithms can be used. A comparison of the optimization algorithms used for that purpose is presented in [4].

The input impedance of helical antennas is around 150 Ω.

Arrays of helical antennas increase the gain compared to a single helical antenna of the same axial length. In addition, by adjusting the array geometry or feeding of array elements, various performances can be achieved [1, 5, 6]. In particular, a planar array with 2×2 elements (a quad array) reduces the width of the main beam of the radiation pattern in both principal planes, yielding a good rotational symmetry of the main beam.

In general, the gain of one optimal nonuniform helical antenna can be about 2.5 dB higher than the gain of a uniform helical antenna of the same axial length. Creating a 2×2 array further increases the gain up to about 6 dB. As an example, using the software WIPL-D [7], we analyzed the quad array of uniform helical antennas presented in [5]. We also designed an array of nonuniform helical antennas of the same axial length (1.5 λ), wire radius, and conductivity. We established that the gain of the quad array of optimal nonuniform antennas can be up to about 2.8 dB higher than the gain of the array of uniform antennas from [5].

In this paper, we present a design of a high-gain quad array of nonuniform helical antennas with an incorporated feeding network, which matches the antenna to 50 Ω. The resulting quad array fits into a box whose dimensions are

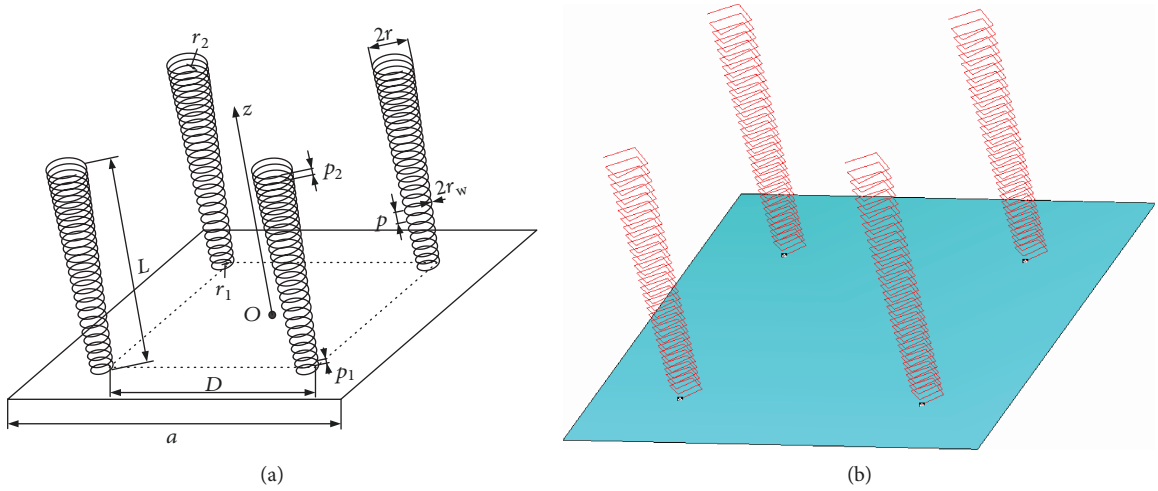

Figure 1: (a) Sketch of the quad array of nonuniform helical antennas and (b) corresponding WIPL-D model.

$2.5 \times 3.3 \times 3.3$ wavelengths, and the gain in the main radiating direction is about 20.5 dBi in the frequency range from 0.9 GHz to 1.1 GHz.

The rest of the paper is organized as follows. Section 2 defines a typical geometry of the considered quad array of helical antennas and presents the corresponding model. Section 3 describes optimization procedures and summarizes the optimal parameters of the antenna geometry. In Section 4, a fabricated prototype of the quad array is presented. Section 5 verifies the presented design through measurements. Section 6 concludes the paper.

2. Geometry and Basic Model of Quad Array of Helical Antennas

The designed quad array of helical antennas consists of four identical (congruent) nonuniform helical antennas, as shown in Figure 1. The antennas are placed above a square ground plane (a reflector) of side a. The feeding points of the antennas are located at vertices of a square of side D (Figure 1(a)). The center of the array coincides with the center of the reflector. In the basic simulation model (Figure 1(b)), all antennas are fed by generators that are of the same rms voltage and in phase. In the final model, a feeding network for the array elements is incorporated as well. Simulations were performed in the software WIPL-D.

Each helical antenna consists of a copper wire bent in the form of a helix (spiral). The wire radius is r_w. The radius r and the pitch p of the helix turns vary linearly along the antenna (i.e., the radius and the pitch are linear functions of the axial coordinate z)

$$r = (r_2 - r_1)\frac{z}{L} + r_1,$$
$$p = (p_2 - p_1)\frac{z}{L} + p_1, \quad (1)$$

where r_1 and p_1 are the radius and pitch of the turn at the helix bottom ($z = 0$), respectively, and r_2 and p_2 are the radius and pitch of the turn at the helix top ($z = L$), respectively (Figure 1(a)).

The operating frequency is 1 GHz; i.e., the free-space wavelength λ is about 300 mm. Each antenna is 2.5 λ long at 1 GHz, i.e., $L \approx 750$ mm. The wire radius is set to $r_w = 0.6\,\text{mm} \approx 0.002\,\lambda$. The surface roughness increases wire losses. Our experience is that, at 1 GHz, this effect can be modeled by taking the wire conductivity to be 2 times lower than that for copper, i.e., $\sigma = 29$ MS/m.

In order to estimate the distance D, we can consider a pair of helical antennas as a uniform antenna array and evaluate the corresponding array factor. The helical antennas in this array are already directive. Hence, the role of the array factor should be to reduce the width of the main beam of these antennas. Intuitively, the first null of the array factor should fall within this main beam.

If D is too small, the null of the array factor approaches the null of the radiation pattern of the helical antennas, the effect of reducing the beamwidth is small, and the increase in the gain is also small. On the other hand, if D is too large, the direction of the null falls too close to the direction of the maximal radiation of the helical antennas and large sidelobes are obtained. Consequently, having in mind the physical limitations for the ground plane, we have optimized D in the range from 400 mm to 600 mm, as it will be explained in the next section.

Since WIPL-D can analyze only straight-line wire segments, each helix turn, of the radius r, is modeled by a square inscribed into a circle whose radius is $r_{out} = 2r/(1 + \cos(\pi/4))$. The circle of the radius r is midway between the inscribed circle and the circumscribed circle of the square. This approximation negligibly changes the simulated gain (for less than 0.1 dB) compared to the gain of an antenna with circular turns or turns approximated by polygons with a very large number of sides. This approximation decreases the computation time. It also simplifies the mechanical structure of the manufactured antenna, which favorably has a relatively small influence on antenna properties.

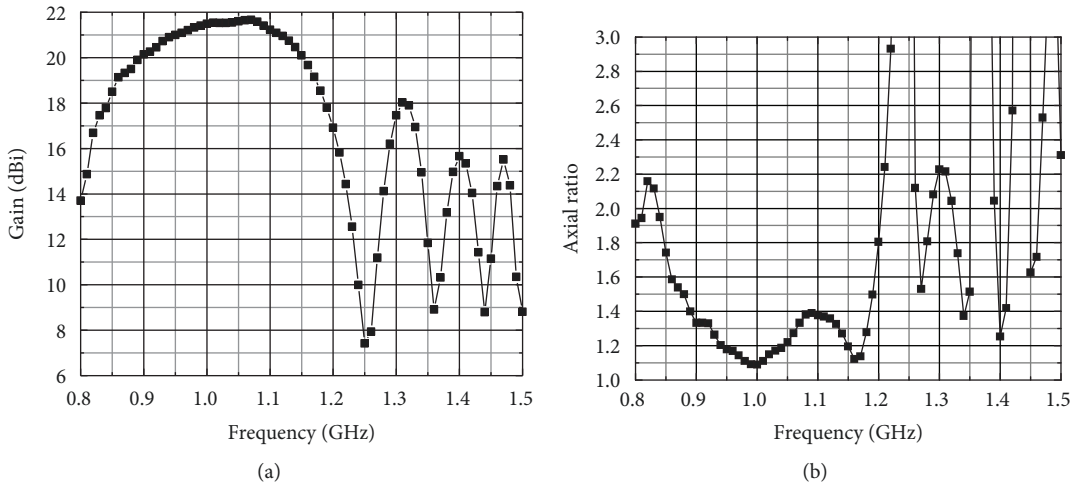

Figure 2: (a) Gain and (b) axial ratio of the optimal quad array.

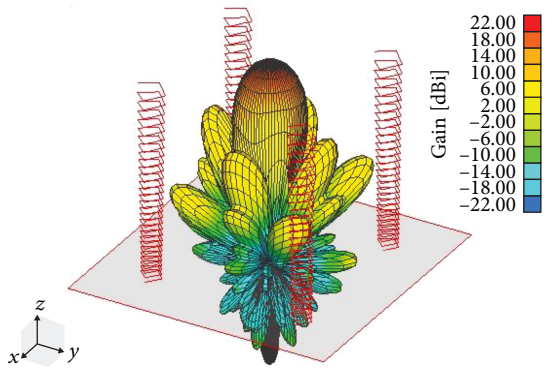

Figure 3: Radiation pattern (3-D) of the optimal quad array at 1 GHz.

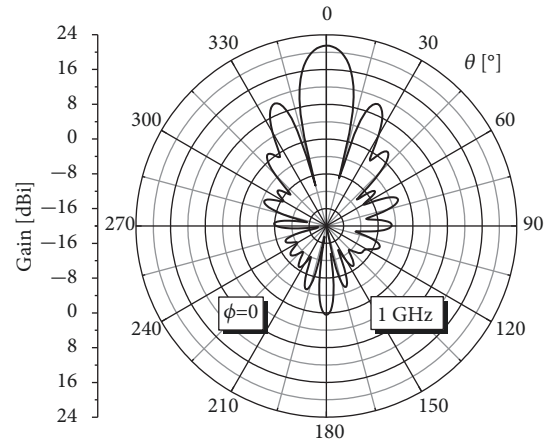

Figure 4: Worst-case ϕ-cut of the radiation pattern at 1 GHz.

3. Optimization Procedure and Optimal Designs

Antenna optimization and design belong to the class of nonlinear programming (NLP) problems. The design (optimization) variables are bounded, as the allowed physical dimensions of the antenna array are limited. Therefore, the design problem is a constrained NLP problem.

Formally, it can be written as $\min f(\mathbf{x})$, $x_{k\,\min} \le x_k \le x_{k\,\max}$, $k = 1, 2, \ldots, M$, where $f(\mathbf{x})$: $\Re^M \longrightarrow \Re$ is the optimization function, M is the total number of optimization variables, $\mathbf{x} = (x_1, x_2, \ldots, x_M)$ is the vector of optimization variables, and $x_{k\,\min}$ and $x_{k\,\max}$ are the lower bound and the upper bound, respectively, of the kth optimization variable. The optimization space S is then a hyperrectangle in the M-dimensional space defined by $x_{k\,\min}$ and $x_{k\,\max}$, $k = 1, 2, \ldots, M$.

The optimization function is the difference between the target electromagnetic (EM) response and the obtained response at x. We use the L_2-norm for the definition of the optimization function. Namely, $f(\mathbf{x}) = \|H(\mathbf{x}) - H_0\|_2 = \sqrt{(H(\mathbf{x}) - H_0)^2}$, where $H(\mathbf{x})$ is the EM response of the antenna at $\mathbf{x}$ and H_0 is the target value of the response. Therefore, the design is transformed into a problem of

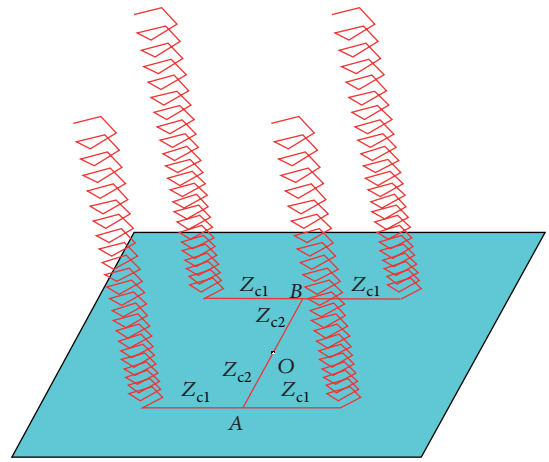

Figure 5: WIPL-D model of the quad array with an H-shaped feeding network.

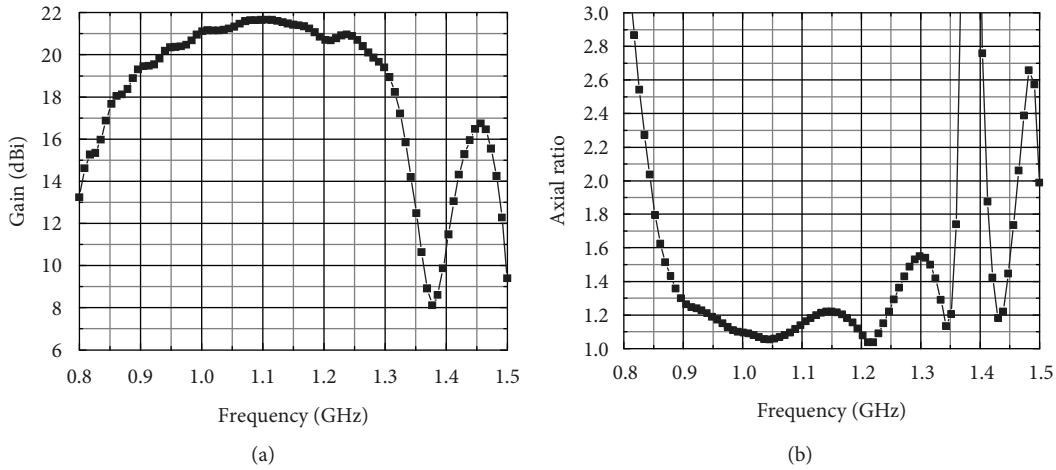

Figure 6: (a) Gain and (b) axial ratio of the optimal quad array with the feeding network.

nonlinear programming, i.e., into finding the minimum of $f(\mathbf{x})$. Note that H_0 should be larger than the maximal possible $H(\mathbf{x})$, so that the best possible design is the global minimum of $f(\mathbf{x})$.

In order to maximize the partial gain for the circular polarization in the main radiating direction at 1 GHz, we optimized the geometry of the quad array using the basic model shown in Figure 1(b). There were $M = 5$ optimization variables:

(i) The radius of the turn at the helix bottom (r_1)

(ii) The radius of the turn at the helix top (r_2)

(iii) The pitch of the turn at the helix bottom (p_1)

(iv) The pitch of the turn at the helix top (p_2)

(v) The distance between the feeding points of the helical antennas (D)

The optimization variables were within the limits:

(i) $25\,\text{mm} \le r_1 \le 40\,\text{mm}$

(ii) $30\,\text{mm} \le r_2 \le 50\,\text{mm}$

(iii) $10\,\text{mm} \le p_1 \le 50\,\text{mm}$

(iv) $10\,\text{mm} \le p_2 \le 50\,\text{mm}$

(v) $400\,\text{mm} \le D \le 600\,\text{mm}$

The optimization was performed using a combination of the random search, the particle swarm optimization (PSO) [8, 9], the Nelder-Mead simplex algorithm [10], and the gradient algorithm [11].

The results of the optimization showed that there were many suboptimal solutions; i.e., there were multiple local minima of the optimization function. Those local minima were found by multiple restarts of local optimization algorithms: the Nelder-Mead simplex or the gradient algorithm. The starting points for the local optimization algorithms were solutions found by multiple restarts of PSO. The initial swarm of PSO was always generated using a random generator with a uniform distribution. The solution having the highest partial gain, found by the optimization, was considered to be the global optimum [4].

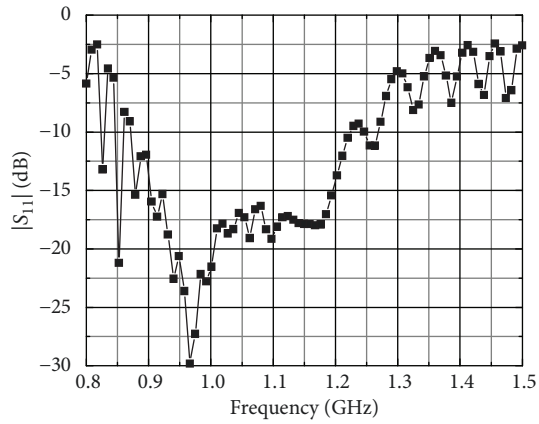

Figure 7: Reflection coefficient at the feeding point of the optimal quad array with the feeding network.

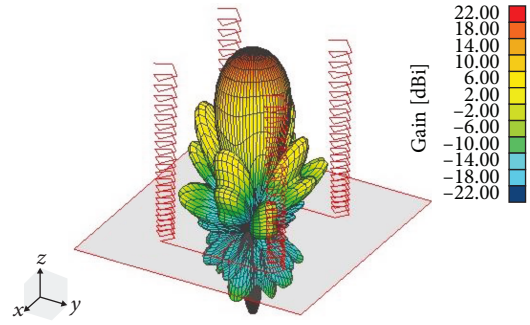

Figure 8: Radiation pattern (3-D) of the optimal quad array with the feeding network at 1 GHz.

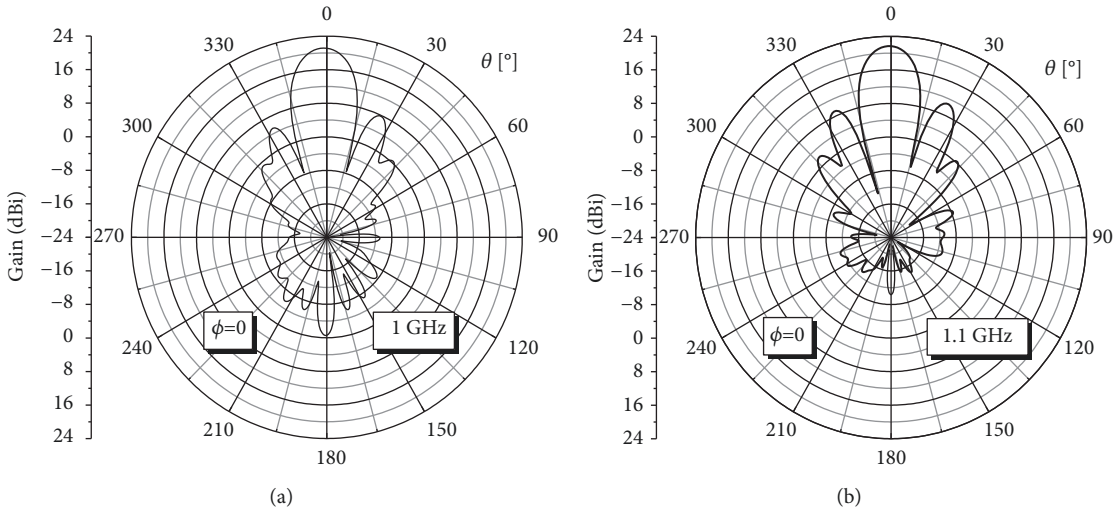

Figure 9: Cuts of the optimal quad array with the included feeding network at $\phi = 0$ (a) at 1 GHz and (b) at 1.1 GHz.

3.1. Optimal Basic Design. For the model shown in Figure 1(b), multiple optimizations yielded practically the same result for the global optimum:

(i) $r_1 = 34.9$ mm

(ii) $r_2 = 47.1$ mm

(iii) $p_1 = 17$ mm

(iv) $p_2 = 37.9$ mm

(v) $D = 586.9$ mm

The gain and the axial ratio of the optimal quad array are shown in Figure 2. The bandwidth of the gain, defined as the frequency band in which the gain is larger than 20 dBi, is almost 25% (from 0.9 GHz to 1.15 GHz). In that range, the axial ratio is smaller than 1.4.

The apparent input impedance (i.e., the ratio of the voltage and the current at the feeding point of a helical antenna) is approximately $Z_{\text{in}} \approx (115 - J20)\Omega$ for all four antennas, in the frequency range from 0.9 GHz to 1.15 GHz.

Figure 3 shows the 3-D radiation pattern of the optimal quad array at 1 GHz. The maximal gain in the main radiating direction is slightly less than 22 dBi. The front-to-back ratio is 21 dB. The ϕ-cut in the worst case ($\phi = 0$) is shown in Figure 4. The largest sidelobes are about 11 dB below the gain in the main direction.

3.2. Optimal Design with a Feeding Network. Further optimization of the geometry of the quad array was performed by incorporating a feeding network that has the shape of letter H (Figure 5). The feeding network consists of six transmission line sections. Each section comprises a copper wire located above the reflector (i.e., the ground plane). The characteristic impedance of the transmission-line sections that interconnect a pair of neighboring helices is Z_{c1}, whereas the characteristic impedance of the two transmission lines in the middle of the feeding network is Z_{c2}, where $Z_{c1} > Z_{c2}$. The section whose characteristic impedance is Z_{c1} transforms the impedance of a single helical antenna. Pairs of those (transformed) impedances are connected in parallel at points A and B. Further, impedances at points A and B are transformed by the transmission lines whose characteristic impedance is Z_{c2}. Finally, two such impedances are connected in parallel at the feeding point (point O in Figure 5). The characteristic impedances Z_{c1} and Z_{c2} were chosen so that the input impedance at the feeding point is as close as possible to 50 Ω (i.e., well matched to a 50 Ω system) in the frequency range from 0.9 GHz to 1.1 GHz.

In the model shown in Figure 5, the characteristic impedances Z_{c1} and Z_{c2} are determined by the elevation of the wire above the reflector and the wire radii. The wire elevation was initially set to 2 mm. The radius of wires that interconnect a pair of neighboring helices was 0.3 mm, and the radius of wires of the two middle sections was 0.6 mm. These radii were chosen because they were commercially available. For these data, the corresponding characteristic impedances are $Z_{c1} = 155\ \Omega$ and $Z_{c2} = 112\ \Omega$.

The next objective was to simultaneously maximize the partial gain for the circular polarization in the main radiating direction and minimize the reflection at the feeding point of the quad array with the incorporated feeding network. Theoretically, this is a two-criterion optimization problem. However, the criteria in our design are weakly coupled and not necessarily in a collision. Namely, the geometry and placement of the nonuniform helical antennas affect the gain and the input impedance of each antenna, while the geometry of the feeding network affects the transformation of the impedance and minimizes the reflection coefficient. The feeding network practically does not radiate, and therefore, it practically does not affect the gain. For those reasons, we opted to combine the two criteria into a single cost function for the optimization, using our engineering experience to estimate the relative weights of the criteria. We organized the optimization so that we were looking for the minimum of the cost function. The optimization was performed for the same set of optimization variables, utilizing the same optimization algorithms as for the basic model.

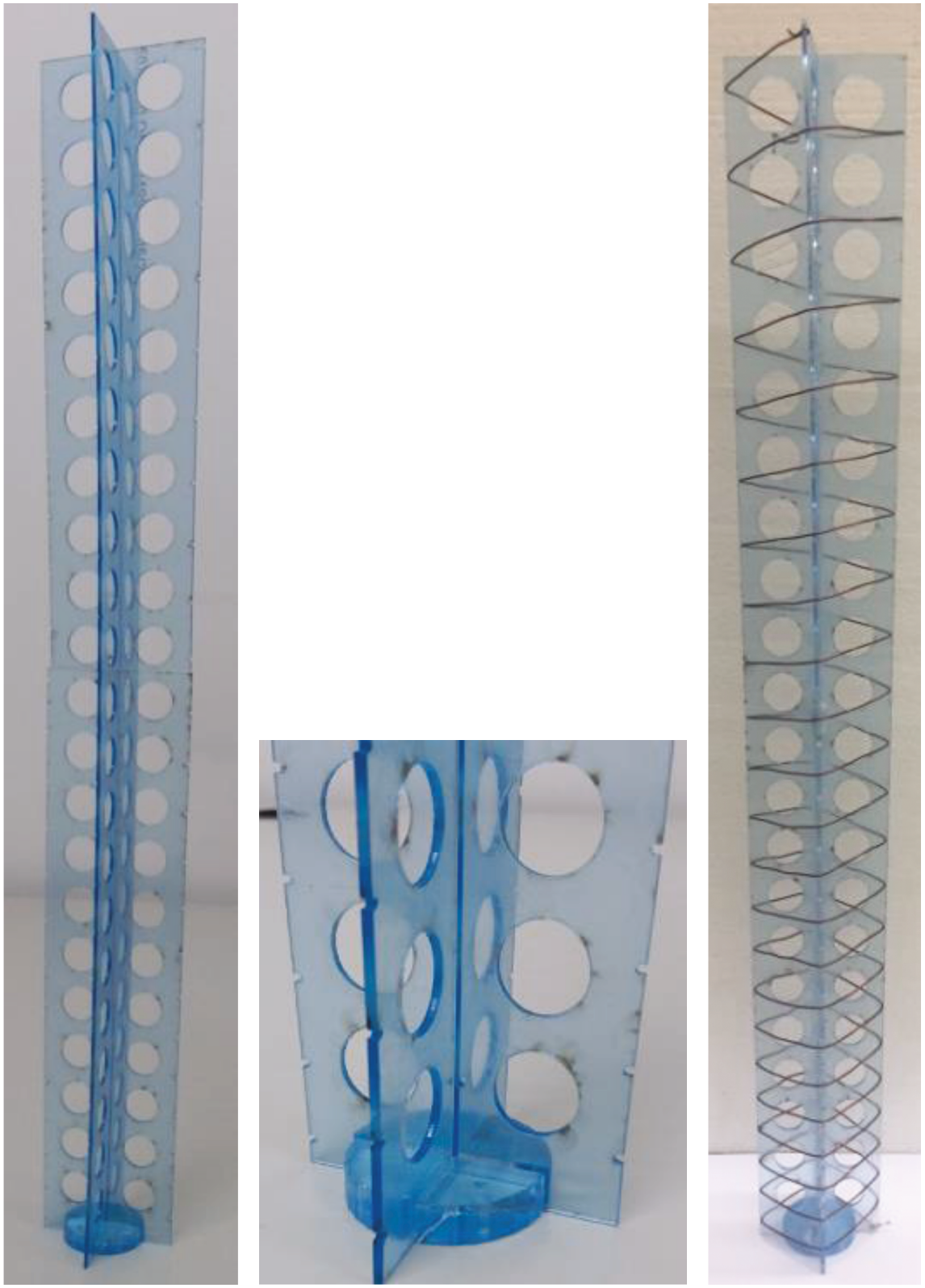

(a) (b) (c)

Figure 10: (a) Acrylic glass wire support, (b) footer, and (c) single helix wound on acrylic glass support.

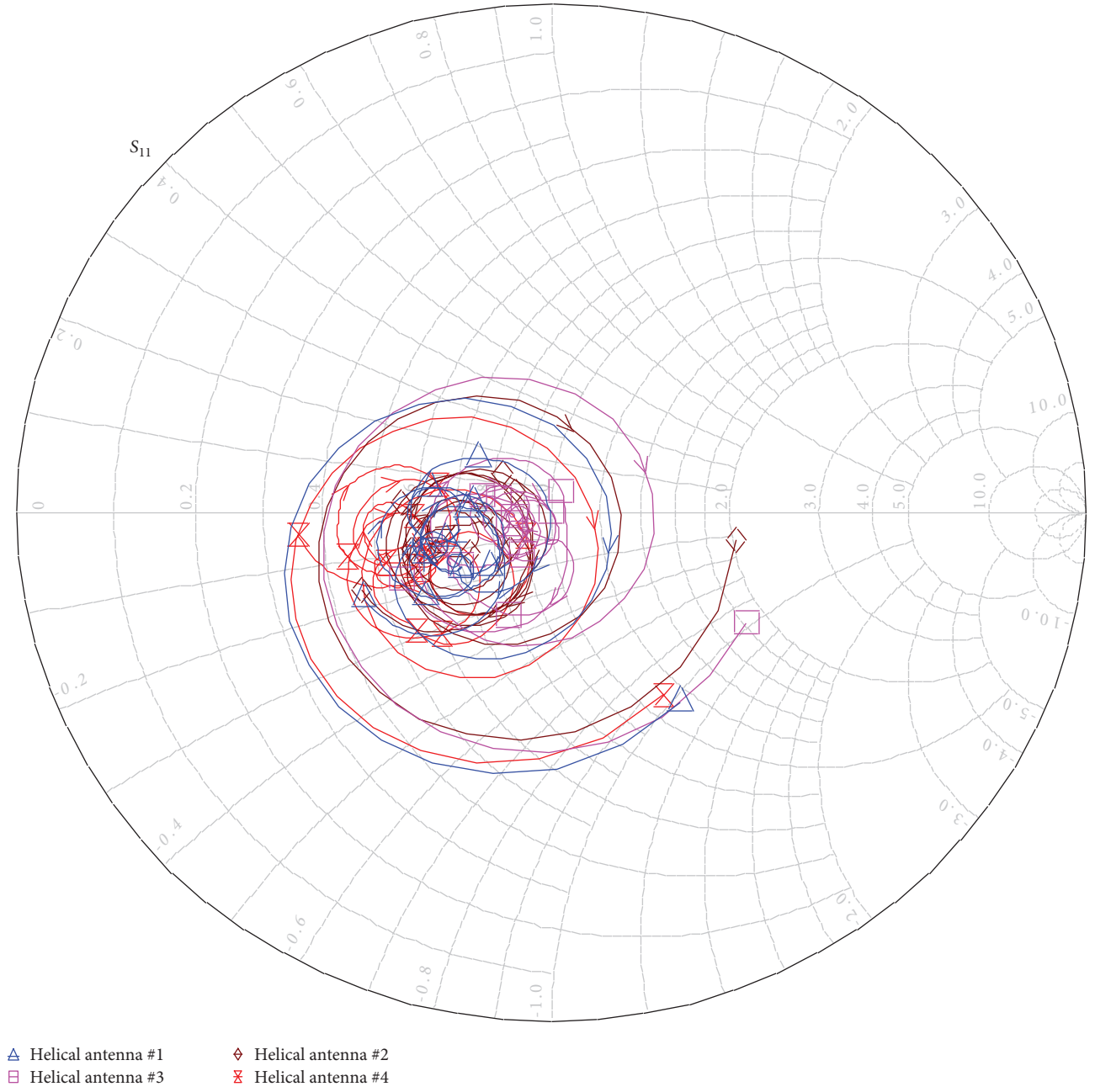

Figure 11: Reflection coefficient of the four helical antennas, with respect to 150 Ω (frequency range from 0.8 GHz to 1.2 GHz).

We considered $N = 5$ equidistantly spaced frequencies within the frequency range from 0.95 GHz to 1.15 GHz, which corresponds to a ~20% bandwidth. The cost function was $f = 1/N\sqrt{\sum_{k=1}^{N}(100 - \text{gain}\,(\text{dBi}))^2} + 1/N\sqrt{\sum_{k=1}^{N}(\max\,(s_{11}\,(\text{dB}) + 15, 0))^2}$, where s_{11} is the reflection coefficient at the antenna feeding point (point O in Figure 5). Note that the considered frequency range was chosen to account for a 5% frequency shift towards lower frequencies due to the imperfect mounting of wires on the supporting structure and the influence of the dielectric of the supporting structure. Therefore, we expected the final antenna to work in the range from 0.9 GHz to 1.1 GHz. The optimal parameters of the antenna with the incorporated feeding network were found to be as follows:

(i) $r_1 = 34.1$ mm

(ii) $r_2 = 44.6$ mm

(iii) $p_1 = 20.5$ mm

(iv) $p_2 = 49.9$ mm

(v) $D = 488.2$ mm

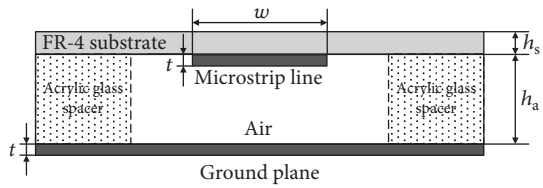

Figure 12: Cross section of the inverted microstrip line.

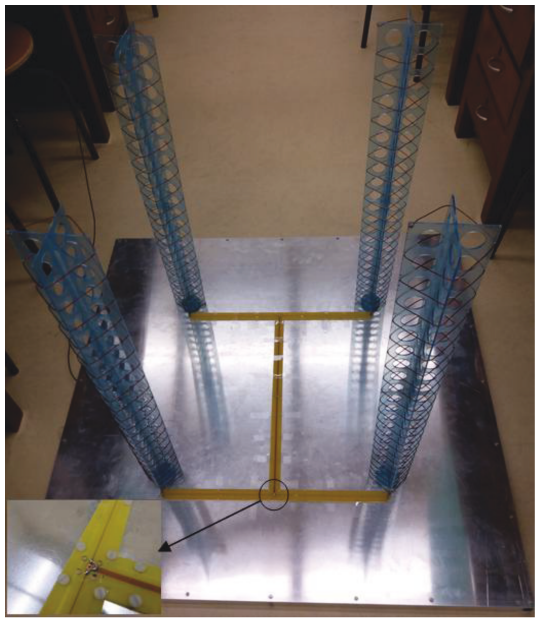

Figure 13: Fully assembled prototype of the quad array.

The gain and axial ratio of the optimal quad array with the feeding network are shown in Figure 6. In this case, the bandwidth is larger, since the optimization was performed in a frequency range. The frequency range where the gain is larger than 20 dBi is from 0.94 GHz to 1.27 GHz, which is almost 33% bandwidth. In this frequency range, the axial ratio is smaller than 1.5.

Simulation results for the reflection coefficient of the optimal quad array with the feeding network are shown in Figure 7. These results indicate that we can obtain a good match of the optimal quad array, with the reflection coefficient below −9.3dB, in the same frequency range in which the gain is larger than 20 dBi.

Figure 8 shows the 3-D radiation pattern of the optimal quad array with the feeding network at 1 GHz, whereas ϕ-cuts at 1 GHz and 1.1 GHz are shown in Figure 9. The presented results, when compared with the results presented in Figures 3 and 4, show that the influence of the feeding network on the radiation pattern is negligible.

4. Prototype of the Quad Array

In order to verify the simulated results, we built a prototype of the quad array. The prototype consists of four nonuniform helical antennas, a ground plane, and a feeding network. The four helical antennas were designed to be identical. However, there were small discrepancies between the antennas due to manual wire winding. Therefore, the feeding network was designed to enable independent testing of each helical antenna, of a pair of the neighboring helices, and of the entire quad array.

A support structure for the helix wire was made of acrylic glass. Acrylic glass was chosen due to its low cost and sufficiently low losses for the presented purpose. The acrylic glass support is shown in Figure 10(a). It was made of three precisely cut acrylic glass panels (each 2 mm thick). These panels were interleaved and fixed together by two small plates (using nylon screws) and gluing. The panels have large holes to reduce their mass. Along the edges of the panels, at precise locations, small grooves were cut in order to hold the wire and to maintain the designed (optimal) radius and pitch of the helix (Figure 10(b)). The antenna has a footer, which consists of four acrylic glass plates whose thickness is

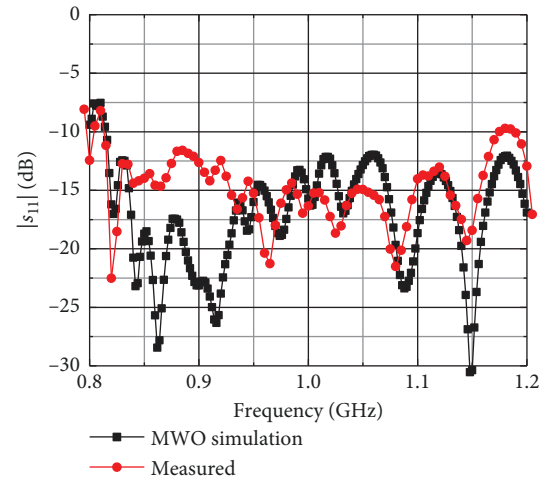

Figure 14: Simulated and measured reflection coefficient of the quad array.

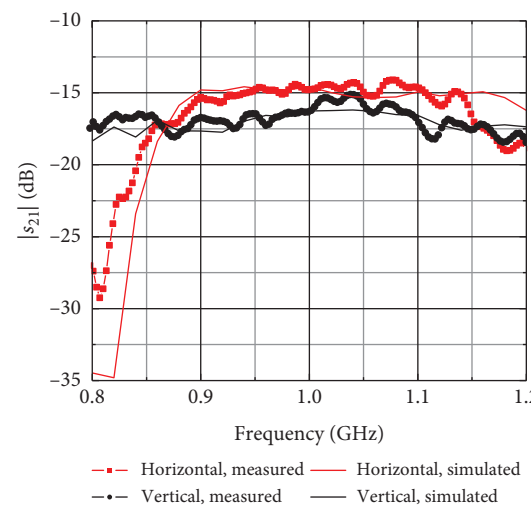

Figure 15: Simulated and measured transmission coefficient between the quad array and Vivaldi antenna for horizontal and vertical polarizations of the electric field.

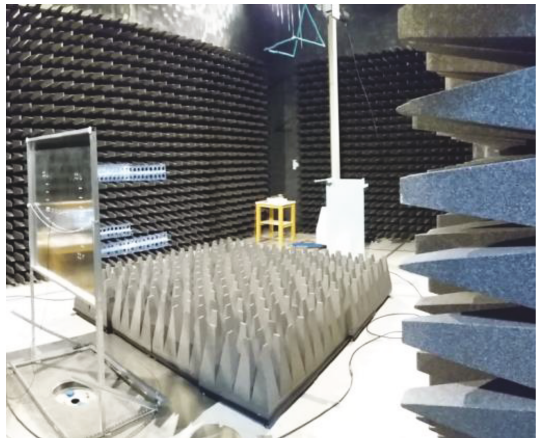

(a)

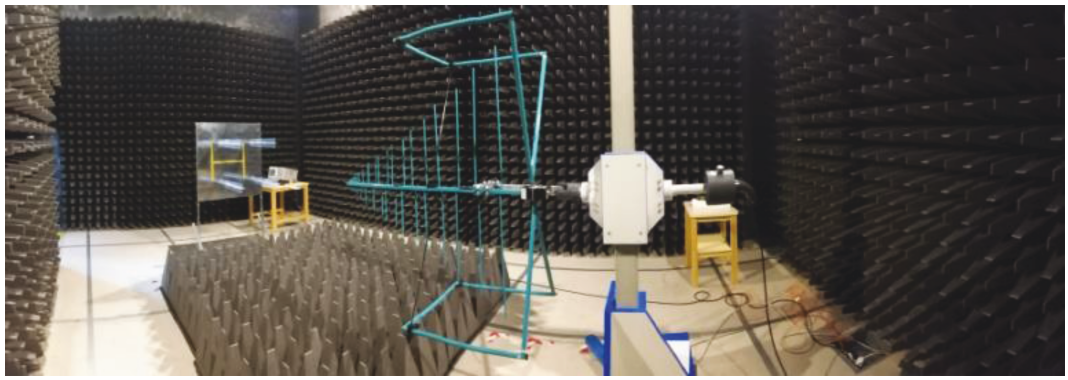

(b)

Figure 16: Measurement setups: (a) quad array and Vivaldi antenna and (b) quad array and BiLog antenna.

10 mm (Figure 10(b)) and which was used for attaching the acrylic glass support to the ground plane. An assembled nonuniform helical antenna is shown in Figure 10(c).

A ground plane for the quad array was designed and manufactured as a square aluminum plate with a side of 1 m and a thickness of 2 mm. The plate has a frame made of aluminum tubes, to increase the rigidity of the structure.

First, we assembled individual helices. The reflection coefficient of each helical antenna was independently measured. Figure 11 shows the reflection coefficients of the four helical antennas with respect to the nominal impedance of 150 Ω in the frequency range from 0.8 GHz to 1.2 GHz. The presented results show that the impedances of the helices are similar to each other.

The transmission lines were made by the printed-circuit technique as inverted microstrip lines. The cross section of the inverted microstrip is shown in Figure 12, where $h_s = 0.5$ mm, $h_a = 2$ mm, and $t = 36\,\mu$m. Microwave Office (MWO) [12] was used to tune the characteristic impedances of the inverted microstrip lines of the feeding network. In this model, the measured scattering parameters of the helical antennas were used. The optimal characteristic impedance of the four inverted microstrip lines connected to the helical antennas was found to be 156 Ω ($w = 0.6$ mm), whereas the optimal characteristic impedance of the remaining two lines was 87 Ω ($w = 3.4$ mm). The resulting input impedance of the quad array at 1 GHz was computed to be about $(38 - J5)\Omega$.

The reason for selecting the inverted microstrip structure was to minimize the influence of the FR-4 substrate [13]. The mechanical stability of the feeding network was achieved by inserting acrylic glass spacers between the FR-4 substrate and the ground plane, running along the edges of the substrate. This sandwich structure was stitched to the ground plane by an array of nylon screws, as shown in the inset of Figure 13.

The fully assembled prototype of the quad array with the feeding network is shown in Figure 13.

Figure 14 shows the simulated reflection coefficient (with respect to 50 Ω) at the feeding point of the complete quad array, including the designed feeding network.

5. Measured Results

In order to experimentally verify the prototype, measurements were performed in the Idvorsky laboratories [14]. The chamber is semianechoic, but additional absorbers were positioned on the floor in order to reduce the wave reflected from the floor. With these additional absorbers, the semianechoic chamber resembles a fully anechoic chamber. The antenna was positioned so that the axes x and z in Figure 8

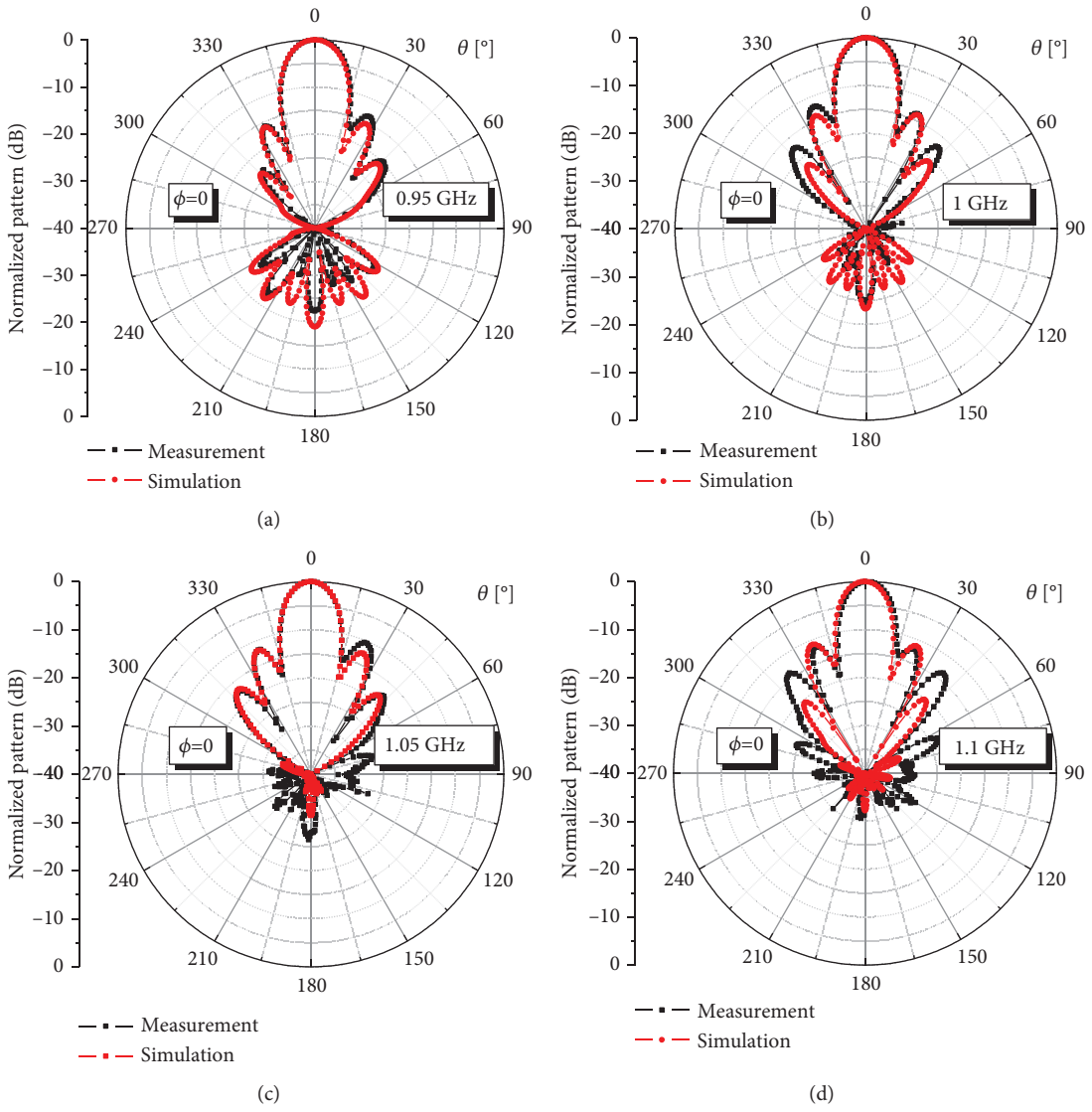

FIGURE 17: Cuts ($\phi = 0$) for the horizontal polarization of the electric field at (a) 0.95 GHz, (b) 1 GHz, (c) 1.05 GHz, and (d) 1.1 GHz.

were horizontal. The center of the ground plane of the quad array was 1320 mm above the floor of the chamber.

The reflection coefficient at the port of the quad array, measured using an Agilent E5061A vector network analyzer (VNA), is shown in Figure 14. The reflection coefficient (with respect to 50 Ω) is lower than −10 dB in the frequency range from 0.81 GHz to 1.17 GHz; i.e., the standing-wave ratio (VSWR) is less than 2.

First, we measured the transmission coefficient between the quad array and the well-documented in-house built Vivaldi antenna, facing each other. The distance between the ground plane of the quad array and the tip of the Vivaldi antenna was 1575 mm, so that the Vivaldi antenna was in the near field of the quad array. The results for the horizontal and vertical polarizations of the electric field are shown in Figure 15. The simulated and measured results for both polarizations agree almost perfectly at 1 GHz. The discrepancy between the simulated and measured results in the frequency range from 0.9 GHz to 1.1 GHz is less than 1.5 dB.

Further, two setups were used for measurements of the radiation pattern of the quad array (Figure 16).

The first setup consisted of the quad array and the Vivaldi antenna (Figure 16(a)). The VNA was connected to both antennas. The distance between the antennas was 4020 mm. The transmission coefficient was both measured and simulated from 0.95 GHz to 1.1 GHz. A comparison of the measured and simulated transmission coefficient, normalized to the maximal level, for the horizontal polarization of the electric field, is shown in Figure 17. The results for the vertical polarization of the electric field, i.e., for the Vivaldi antenna rotated for 90 degrees, are shown in Figure 18.

In the second measurement setup, shown in Figure 16(b), a signal generator Rohde & Schwarz SML03 (whose power level was 0 dBm at 0.99 GHz) was connected to the quad

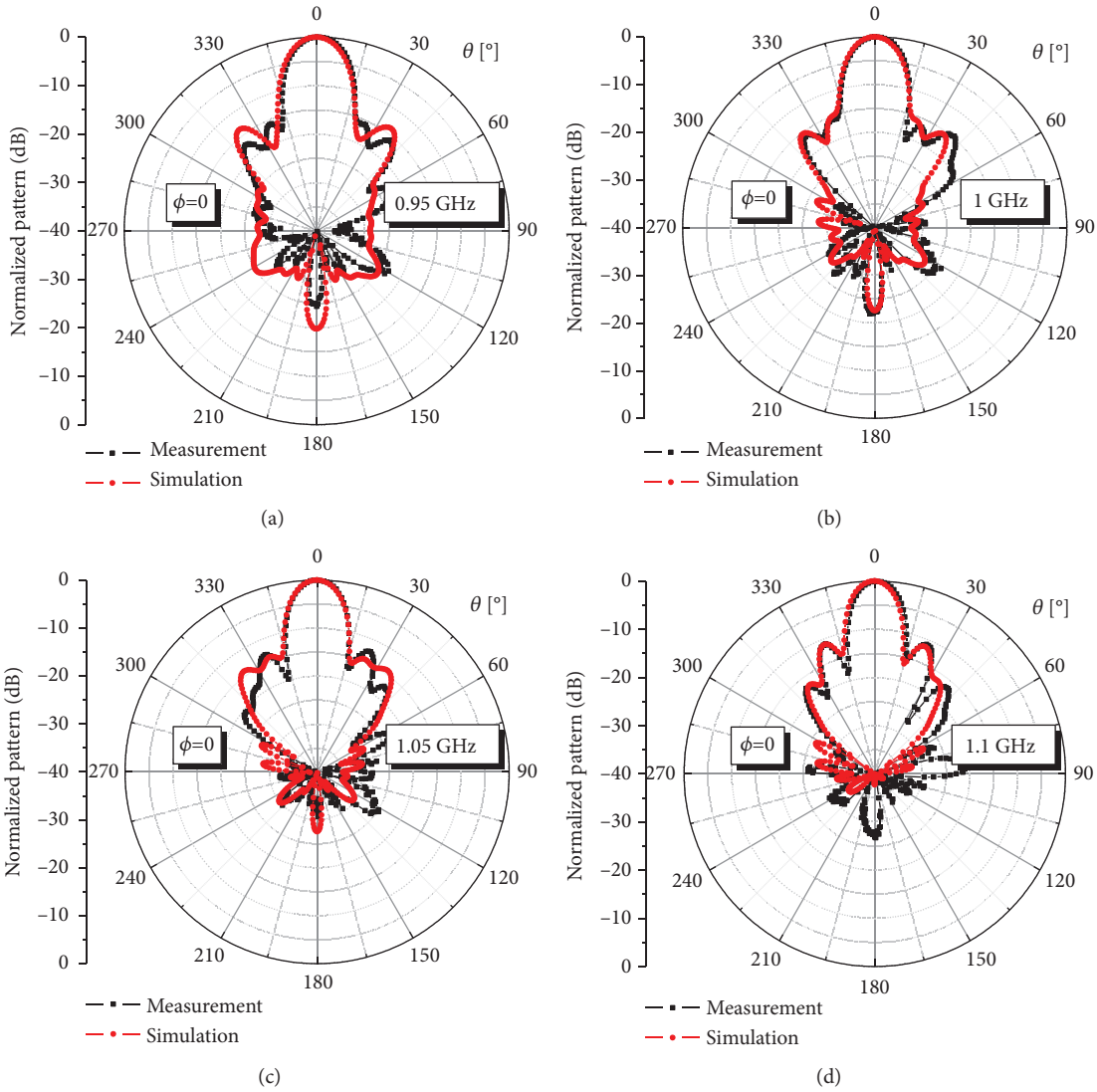

Figure 18: Cuts ($\phi = 0$) for the vertical polarization of the electric field at (a) 0.95 GHz, (b) 1 GHz, (c) 1.05 GHz, and (d) 1.1 GHz.

array, while the receiving antenna was a Teseq CLB 6144 BiLog antenna. Using a Teseq SMR4503 EMI receiver, the electric field was measured at a 3000 mm distance. The results for the electric field level, normalized to the maximal level, are shown in Figure 19.

A question arises if the measurement distances of 3000 mm and 4020 mm are sufficient for obtaining valid far-field patterns for the quad array. To answer the question, we calculated (using the WIPL-D software) the electric field in the far field and at the 3 m and 4 m distances from the quad array. We compared the normalized electric fields in these cases for different angles θ. Almost perfect agreement was obtained for the main lobe. The levels of the major sidelobes and most nulls were larger in the near-field model. However, we considered these discrepancies to be within acceptable limits, in particular because our focus was on the main lobe and the maximal antenna gain.

From all the results presented in this section, we conclude that the radiation pattern of the quad array prototype closely resembles the designed one. The gain in the main radiation direction at 1 GHz is 21 dBi, whereas in the frequency range from 0.9 GHz to 1.1 GHz, the gain is 20.5 ± 1.5 dBi.

6. Conclusions

The paper presents a design procedure of a high-gain quad array of nonuniform helical antennas. We started from the optimal design of a single helical antenna. Further, we optimized the geometry of the quad array of identical helical antennas using various optimization algorithms. The optimal geometry of the quad array was obtained with an incorporated feeding network, which was also used for matching the port of the quad array to 50 Ω. Finally, the presented design was verified by measurements of the fabricated prototype of the quad array. The gain of the designed quad array is 20.5 ± 1.5 dBi in the frequency range from 0.9 GHz to 1.1 GHz. In the considered frequency range, the reflection

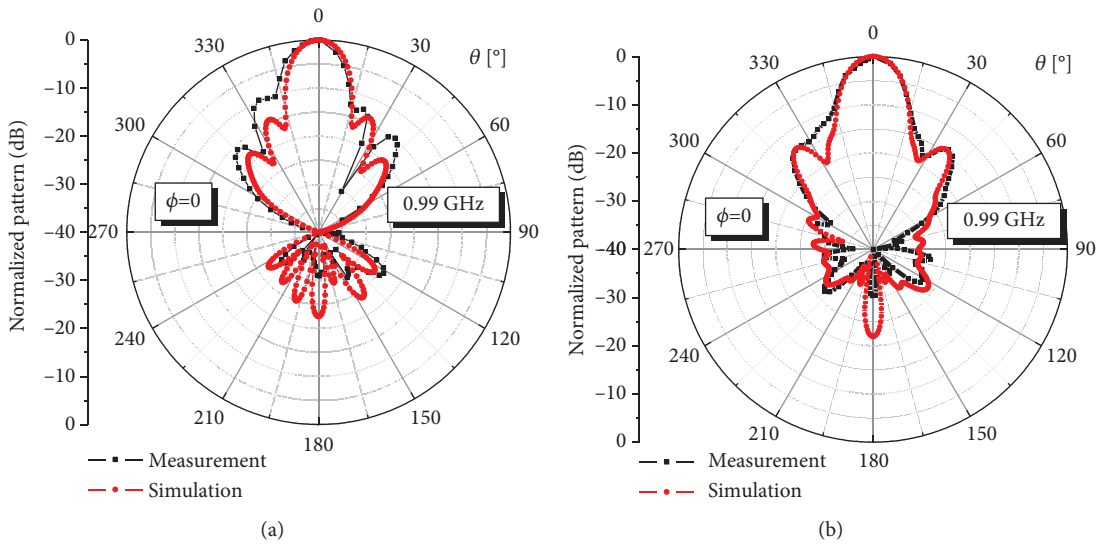

Figure 19: Normalized level of (a) horizontal and (b) vertical component of the electric field at 0.99 GHz and 3000 mm distance.

coefficient (with respect to 50 Ω) is less than −12.4 dB. The designed quad array fits into a box whose dimensions are $2.5 \times 3.3 \times 3.3$ wavelengths.

Data Availability

The complete data for the geometry and materials of the designed and produced high-gain quad array of nonuniform helical antennas, used to support the findings of this study, are included within the article.

Disclosure

The views and findings in this paper are those of the authors and do not necessarily reflect the views of DARPA.

Conflicts of Interest

The authors declare that there is no conflict of interest regarding the publication of this paper.

Acknowledgments

This work was supported in part by Defense Advanced Research Projects Agency LADS contract FA8650-16-C-7620.

References

[1] J. D. Kraus, "The helical antenna," in *Antennas, Chapter 7*, pp. 265–339, McGraw-Hill, New York, NY, USA, 1988.

[2] A. R. Djordjević, A. G. Zajić, M. M. Ilić, and G. L. Stüber, "Optimization of helical antennas," *IEEE Antennas and Propagation Magazine*, vol. 48, no. 6, pp. 107–115, 2006.

[3] R. Golubovic, A. Djordjevic, D. Olcan, and J. Mosig, "Non-uniformly-wound helical antennas," in *2009 3rd European Conference on Antennas and Propagation*, pp. 3077–3080, Berlin, Germany, March 2009.

[4] J. L. Dinkić, D. I. Olćan, A. G. Zajić, and A. R. Djordjević, "Comparison of optimization approaches for designing nonuniform helical antennas," in *2018 IEEE International Symposium on Antennas and Propagation & USNC/URSI National Radio Science Meeting*, pp. 1581-1582, Boston, MA, USA, 2018.

[5] J. Zemanovič, P. Hajach, and P. Podhoranský, "Verification of four elements helical antennas array design procedure," in *2008 14th Conference on Microwave Techniques*, pp. 1–4, Prague, Czech Republic, 2008.

[6] S. I. S. Hassan, M. F. Ain, and A. R. Arief, "Four beams helical antenna array for mobile satellite application," in *2004 RF and Microwave Conference*, pp. 53–55, Subang, Selangor, Malaysia, October 2004.

[7] WIPL-D, *WIPL-D Pro v15.0—3D EM Solver*, WIPL-D, Belgrade, Serbia, 2018, http://www.wipl-d.com.

[8] J. Kennedy and R. Eberhart, "Chapter seven-the particle swarm," in *Swarm Intelligence*, pp. 287–326, Morgan Kaufmann, 2001.

[9] J. Robinson and Y. Rahmat-Samii, "Particle swarm optimization in electromagnetics," *IEEE Transactions on Antennas and Propagation*, vol. 52, no. 2, pp. 397–407, 2004.

[10] J. A. Nelder and R. Mead, "A simplex method for function minimization," *The Computer Journal*, vol. 7, no. 4, pp. 308–313, 1965.

[11] D. P. Bertsekas, *Convex Optimization Algorithms, Chapter 2.1*, Athena Scientific, 2015, 64.

[12] http://www.awrcorp.com.

[13] B. E. Spielman, "Dissipation loss effects in isolated and coupled transmission lines," *IEEE Transactions on Microwave Theory and Techniques*, vol. 25, no. 8, pp. 648–656, 1977.

[14] http://www.idvorsky.com/en/.